

A 4D Hybrid Algorithm to Scale Parallel Training to Thousands of GPUs

Siddharth Singh, Prajwal Singhania, Aditya K. Ranjan, Zack Sating, Abhinav Bhatele

Department of Computer Science
University of Maryland

E-mail: {ssingh37, prajwal, aranjn2, zsating}@umd.edu, bhatele@cs.umd.edu

Abstract—Heavy communication, in particular, collective operations, can become a critical performance bottleneck in scaling the training of billion-parameter neural networks to large-scale parallel systems. This paper introduces a four-dimensional (4D) approach to optimize communication in parallel training. This 4D approach is a hybrid of 3D tensor and data parallelism, and is implemented in the AxoNN framework. In addition, we employ two key strategies to further minimize communication overheads. First, we aggressively overlap expensive collective operations (reduce-scatter, all-gather, and all-reduce) with computation. Second, we develop an analytical model to identify high-performing configurations within the large search space defined by our 4D algorithm. This model empowers practitioners by simplifying the tuning process for their specific training workloads. When training an 80-billion parameter GPT on 1024 GPUs of Perlmutter, AxoNN surpasses Megatron-LM, a state-of-the-art framework, by a significant 26%. Additionally, it achieves a significantly high 57% of the theoretical peak FLOP/s or 182 PFLOP/s in total.

Index Terms—Parallel deep learning, Tensor parallelism, Communication modeling, Asynchronous communication

I. INTRODUCTION

The effectiveness of deep learning (DL) models at generalization improves reliably with an increase in their number of parameters [1], [2]. This trend has led to the development of large foundational models trained using deep neural networks (DNNs) with hundreds of billions of parameters [3], [4]. Given the substantial memory requirements for training these models, which often exceeds the memory capacity of single server-class GPUs, the use of GPU-based clusters for model training has become common. Consequently, it is imperative to develop efficient parallel algorithms and frameworks that can leverage the combined memory capacity and computational power of hundreds to thousands of GPUs for efficient training of such neural networks.

The foremost challenge in scaling parallel DL training across multi-GPU clusters is communication. While modern GPUs have significantly improved compute efficiency due to their use of specialized cores such as Tensor Cores in NVIDIA GPUs, network bandwidth across compute nodes has lagged behind. This results in modern frameworks for parallel DL training being inefficient at scale due to the considerable overhead of message passing. These overheads stem primarily from two factors: (i) the inherently large communication volume associated with the underlying parallel DL algorithms,

and (ii) inefficient use of message passing with minimal to no overlap with computation. These communication challenges deteriorate the efficiency of parallel frameworks, becoming progressively more severe as we scale to thousands of GPUs. Unfortunately, scalability is increasingly crucial due to the compute-intensive nature of modern training workloads such as large language models (LLMs).

To overcome challenges (i) and (ii), we propose a four-dimensional (4D) hybrid parallel algorithm, implemented in AxoNN, a framework for parallel DL training. This 4D approach is a hybrid of 3D tensor and data parallelism. We use a variation of Agarwal et al.’s parallel matrix multiplication algorithm [5] to efficiently parallelize the compute-intensive matrix multiplications within each layer of the neural network. This is often referred to as tensor parallelism. While utilizing an efficient parallel matrix multiplication algorithm is a crucial step, there are other factors needed to achieve communication efficiency. To further improve performance, we employ the following two approaches.

Overlapping Communication and Computation: Many tensor parallel approaches, including the one proposed in this work, rely on collective communication operations (reduce-scatter, all-gather, and all-reduces). These operations can be expensive at scale in terms of performance. To address scalability issues, we propose several communication optimizations that leverage asynchronous communication primitives, while being mathematically equivalent to the synchronous implementation. These primitives allow for significant overlap between communication and computation, maximizing hardware utilization.

Communication-aware Configuration Selection: Our 4D algorithm requires arranging the available GPUs in a virtual 4D grid and deciding the sizes of each dimension. The distribution of data and compute work on this virtual 4D grid can significantly impact communication costs. To assist users, we introduce a model that identifies a small set of communication-optimal configurations for a given DL workload, eliminating the need to explore the entire search space of possible values for each of the 4 dimensions. Rather, users can profile these suggested configurations, streamlining the process of finding the optimal settings for their specific workload.

We demonstrate the performance of our framework by conducting scaling studies on multi-billion parameter DNNs,

then comparing our performance with three state-of-the-art parallel deep learning frameworks – Megatron-LM [6] and DeepSpeed-3D [7], and ZeRO-3 [8], on both the Perlmutter (Nvidia A100 GPUs) and Frontier (AMD MI250X GPUs) supercomputers. In a weak scaling study using GPT-3 transformer models ranging 5B-80B parameters over 64-1024 GPUs, we observe significant performance improvements of 25–45% over Megatron-LM and 32–50% over DeepSpeed-3D on Perlmutter, and 23–35% over DeepSpeed-3D on Frontier. We demonstrate that AxoNNscales well, even on AMD GPUs, where other frameworks struggle. We also show significant improvements when training vision models (UNet CNNs) in a weak scaling study when compared to ZeRO-3 [8].

In summary, we make the following contributions:

- An open-source, 4D tensor + data hybrid parallel framework, AxoNN, which reduces communication overhead and speeds up DNN training at scale, compared to other state-of-the-art frameworks.
- Techniques for optimizing collective communication by leveraging asynchrony and intelligent communication scheduling, which maximize overlap between computation and communication.
- A performance model for communication, tailored to assist users in discovering communication-minimizing configurations for AxoNN.

II. RELATED WORK

In this section, we present related work on different frameworks and algorithms for parallel deep learning training, primarily focusing on tensor parallelism and communication performance modeling.

A. Tensor Parallelism

Tensor parallel algorithms work by parallelizing the computation of every layer of the neural network. Most frameworks for tensor parallelism focus on fully-connected (FC) and/or convolutional layers. The most widely used tensor parallel framework is Shoeybi et al.’s Megatron-LM [6]. In their work the authors propose an algorithm to parallelize a pair of FC layers. They apply their technique to parallelize large GPT style transformers efficiently within GPUs in a node.

Qifan et al. propose a 2D tensor parallel algorithm for FC layers [9] based on the SUMMA algorithm for distributed matrix multiplication. Similarly, Wang et al. propose a 2.5D parallel algorithm for FC layers [10]. Perhaps the closest algorithm to our work is Bian et al.’s 3D tensor parallel algorithm [11], which is also based on Agarwal’s 3D matrix multiplication algorithm. However, (i) the authors do not propose any communication overlap optimizations like we do in Section IV, and (ii) they do not provide any discussion on choosing the optimal 3D configurations for their algorithm and instead heuristically opt for symmetric cubic configurations. As we show in Section V, arriving upon optimal/near-optimal configurations is very critical for performance. Also they only show results on single layers, whereas we demonstrate results

on full fledged multi-billion parameter models on 1000s of GPUs.

Jangda et al. develop high performance GPU kernels that overlap computation with communication in Megatron-LM’s algorithm [12]. Dryden et al. propose channel and filter parallelism for convolution layers [13]. Wang et al. propose using asynchronous sends instead of all-gather operations for a 2D tensor parallel scheme to overlap communication and computation [14]. Merak [15] introduces an automated 3D parallel framework based on graph partitioning, along with techniques to overlap communication with computation in pipeline and tensor parallelism modes. Li et al. propose Oases, which overlaps backward pass communication with activation recomputation [16].

B. Modeling Communication Performance

In order to alleviate the complexity of choosing the correct mapping of GPUs to the different parallelism dimensions, several works have proposed automated frameworks that try to model the behavior of the configurations with respect to the communication and computation costs.

Alpa [17] is a compiler that automates the process of parallelizing neural networks by coming up with communication efficient strategies for decomposing a given set of GPUs into a hybrid 1D tensor, pipeline and data parallelism scheme. However, (i) they only model a 1D tensor parallel approach, whereas our communication model accounts for a 3D tensor parallel paradigm (see Section V), and (ii) their communication model is placement-agnostic and only models the communication volume. In contrast, the communication model proposed in this work is placement-aware and accounts for variations in bandwidths depending on the mapping of the process groups to the underlying topology.

Cheng et al. develop a hierarchical communication matrix over a 2-dimensional device mesh to model the communication cost [18], taking the underlying network topology into account, and use it to automate the decomposition over a 2D tensor parallelism scheme. Li et al. extend Alpa and model the cost of overlapped communication-computation for improving the automated parallel plan [16]. Alok et al. propose parallel algorithms and model communication costs for training Graph Neural Networks [19].

III. DESIGNING A HYBRID 3D TENSOR AND DATA PARALLEL FRAMEWORK

In this section, we describe our new approach to scaling the training of large multi-billion parameter neural networks to thousands of GPUs. We have designed a hybrid parallel approach that combines 3D tensor and data parallelism. Below, we describe both components, starting with data parallelism.

A. Data Parallelism

Let us assume that we want to parallelize training on G GPUs. When using only data parallelism, we first instantiate a full copy of the neural network on every GPU, and then divide the input batch into equal-sized *shards* among these

GPUs. However, since we want to use a hybrid approach that combines data with tensor parallelism, we first organize the total number of GPUs, G , into a virtual 2D grid, $G_{\text{data}} \times G_{\text{tensor}}$. This results in G_{data} groups of G_{tensor} GPUs each. We use data parallelism across the G_{data} groups, and tensor parallelism within each group. Similar to pure data parallelism, the G_{data} groups in hybrid parallelism also have to synchronize their weights by issuing all-reduces on their gradients after every batch.

B. Three-dimensional Tensor Parallelism

Next, we describe how each GPU group, composed of G_{tensor} GPUs, parallelizes the work within their copy of the neural network. Each GPU group processes the batch shard assigned to them. Tensor parallelism refers to parallelizing the computation within every layer of the neural network across GPUs. We first describe the parallelization of a single layer using our approach. We use the fully-connected (FC) or Linear layer as an example.

Let us first look at the serial computation in an FC layer. Each FC layer computes one half-precision matrix multiplication in the forward pass and two half-precision matrix multiplications in the backward pass. The inputs to the matrix-multiply (MM) kernel in the forward pass are the input activation, I , and the layer’s weight matrix, W . The output of the MM operation is the output activation, O . This is illustrated in Figure 1. In the backward pass, there are two MM operations, $\frac{\partial L}{\partial O} \times W^T$ and $I^T \times \frac{\partial L}{\partial O}$, where L is the training loss. Thus, parallelizing an FC layer requires parallelizing these three MM operations across multiple GPUs.

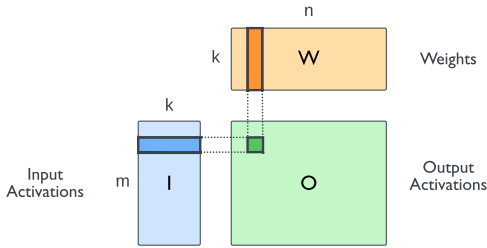


Fig. 1: Computation in the forward pass of a fully-connected (FC) layer with input I and layer weights W . The output, O is a matrix multiplication of I and W . We assume $I \in \mathbb{R}^{m \times k}$, $W \in \mathbb{R}^{k \times n}$, and $O \in \mathbb{R}^{m \times n}$.

In order to parallelize a single matrix-multiply computation across several GPUs, we adapt Agarwal et al.’s 3D parallel matrix multiplication algorithm [5]. As noted in Section III-A, we need to exploit G_{tensor} GPUs for tensor parallelism within each group. Since Agarwal’s algorithm uses a virtual 3D grid of processes, we first organize the G_{tensor} GPUs further into a virtual three-dimensional (3D) grid of dimensions $G_x \times G_y \times G_z$. As an example, we show a topology of eight GPUs with $G_x = G_y = G_z = 2$ in Figure 2. Additionally, we use $g_{i,j,k}$ to refer to a GPU in the grid.

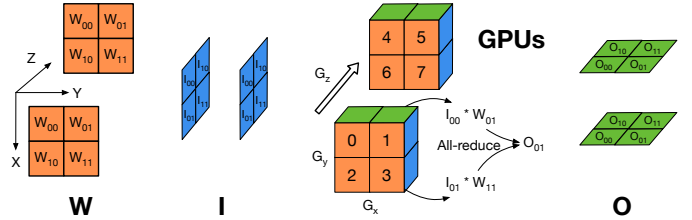


Fig. 2: Parallelization of an FC layer with Agarwal’s 3D parallel matrix multiplication algorithm [5] on eight GPUs organized in a $2 \times 2 \times 2$ topology. We use G_x , G_y , and G_z to refer to the number of GPUs along the three dimensions of the virtual grid topology.

Now let us discuss how we use Agarwal’s algorithm to distribute input activations, I , and weights, W , onto this 3D grid of GPUs. We do 2D decompositions of both I and W into sub-blocks and map them to orthogonal planes of the 3D grid. For example, in Figure 2, we observe that W is partitioned along the X and Y -axes, and replicated along the Z -axis. This means that GPU groups in each XY plane have a copy of W . The I matrix on the other hand is partitioned along the X and Z -axes, and replicated along the Y -axis. Once each GPU has a unique sub-block of I and W , it can compute a portion of the O matrix, which can be aggregated across GPUs in the Y direction using all-reduces.

In our adapted version of Agarwal’s algorithm, instead of replicating W along the Z -axis, we further shard W along the Z -axis and denote these sub-shards as \hat{W} . This is done to save memory as the set of GPUs along the Z -axis will only have to store the gradients and optimizer states of unique shards of the weights. We now discuss how we adapt Agarwal’s algorithm to work with sharded weight matrices in the forward and the backward passes of our 3D tensor parallel algorithm. We illustrate the forward pass in function `TENSOR_PARALLEL_FORWARD_PASS` of Algorithm 1 from the perspective of GPU $g_{i,j,k}$.

The inputs to this function are $I_{k,j}$ and $\hat{W}_{j,i}$ i.e. the shards of I and W mapped to GPU $g_{i,j,k}$ by our algorithm. Since we have performed an extra sharding of W along the Z -axis, we first bring back the full required sub-block of W by issuing an all-gather on \hat{W} ’s to get W (line 2). Then, every GPU computes a matrix multiply of their local partitions of the input activations and weights, which is $I_{k,j} \times W_{j,i}$ (line 3). However, since the columns of I are distributed across the GPUs along the Y -axis, this step requires an all-reduce operation within the Y - tensor parallel GPUs to compute the complete output (line 4). Finally, at the end of the forward pass, each GPU caches its local partitions of I and W , as these are required in the backward pass (line 5).

Let us now discuss the parallelization in the backward pass. $\frac{\partial L}{\partial O_{k,i}}$ is the partial derivative of the loss with respect to the output of the forward pass, which serves as the input to the backward pass. First, we retrieve the local partitions of the data, which we had cached earlier in the forward pass (line

Algorithm 1 Our 3D tensor parallelism for $g_{i,j,k}$ in a $G_x \times G_y \times G_z$ grid. We highlight all communication operations in blue.

```

1: function TENSOR_PARALLEL_FORWARD_PASS( $I_{k,j}, \hat{W}_{j,i}$ )
2:    $W_{j,i} = \text{ALL-GATHER}_z(\hat{W}_{j,i})$ 
3:    $\hat{O}_{k,i} = I_{k,j} \times W_{j,i}$ 
4:    $O_{k,i} \leftarrow \text{ALL-REDUCE}_y(\hat{O}_{k,i})$ 
5:   // Cache  $I_{k,j}$  and  $W_{j,i}$  for the backward pass
6:   return  $O_{k,i}$ 
7: end function
8:
9: function TENSOR_PARALLEL_BACKWARD_PASS( $\frac{\partial L}{\partial O_{k,i}}$ )
10:  Retrieve  $I_{k,j}$  and  $W_{j,i}$  from cache
11:   $\frac{\partial L}{\partial I_{k,j}} \leftarrow \text{ALL-REDUCE}_x(\frac{\partial L}{\partial O_{k,i}} \times W_{j,i}^\top)$ 
12:   $\frac{\partial L}{\partial \hat{W}_{j,i}} \leftarrow \text{REDUCE-SCATTER}_z(I_{k,j}^\top \times \frac{\partial L}{\partial O_{k,i}})$ 
13:  return  $\frac{\partial L}{\partial I_{k,j}}, \frac{\partial L}{\partial \hat{W}_{j,i}}$ 
14: end function

```

10). After this step, we have all the data in place to begin computing the two matrix multiplications in the backward pass. We start with computing the gradients of the loss with respect to I i.e. $\frac{\partial L}{\partial I} = \frac{\partial L}{\partial O} \times W^\top$. For this, each GPU does a matrix multiplication, $\frac{\partial L}{\partial O_{k,i}} \times W_{j,i}^\top$ (line 11). Just like the forward pass, this results in a partial output which needs to be aggregated via an all-reduce. However, in this case the all-reduce is done by GPUs along the X -axis (line 11). Next, we compute the derivative with respect to the weights by multiplying the transpose of the local partition of I with the local partition of $\frac{\partial L}{\partial O}$ i.e. $I_{k,j}^\top \times \frac{\partial L}{\partial O_{k,i}}$. Finally, we do a reduce-scatter on the outputs so that each GPU ends up with the gradients of their shard of the weights (line 12).

Extension to convolution layers: Algorithm 1 can be easily extended to convolution layers by treating k and n as the number of input and output channels, respectively.

Parallelizing an entire network: Consider a simple neural with two FC layers parallelized using Algorithm 1. The output O of the first layer would be the input to the other. However, notice in Figure 2 how O is divided across the 3D tensor parallel grid differently than the input I . So to ensure that the second layer can work with O we would need to transpose its weight matrix – essentially dividing its rows across the X -axis and columns across the Y -axis. This transpose needs to be done once at the beginning of training. So, to parallelize a full neural network, we simply ‘transpose’ the weights of every alternate layer by swapping the roles of the X - and Y -tensor parallel groups.

IV. PERFORMANCE OPTIMIZATIONS IN AXONN

In this section, we present communication optimizations that target the reduction of communication time for a given training workload, consisting of the neural network, its hyper parameters, and the number of GPUs, along with a predefined

set of values for the configurable performance parameters of our algorithm. As a running example, we consider a 20B parameter GPT style transformer [3] with a batch size of 32k tokens (sequence length of 2k tokens) on 16 GPUs or four nodes of the Perlmutter supercomputer. We use a configuration of $G_x = 2, G_y = 2, G_z = 4$, and $G_{data} = 1$

A. Overlapping All-Reduces with Computation

This optimization is concerned with overlapping the all-reduce communication in the backward pass of a layer across the X -tensor parallel group (Line 11 of Algorithm 1) with computation. Note that for layers with ‘transposed’ weight matrices discussed in the previous section, this communication would happen across the Y -tensor parallel groups. Our strategy to achieve overlap is to issue the all reduce in line 11 asynchronously and overlap it with the computation of the weight gradients happening in line 12. Once this computation has finished, we wait on the asynchronous all reduce to finish. From Figure 3, we can see that adding this optimization increases the proportion of communication overlapped with computation, improving batch times by around 5%.

Breakdown of Batch Times for GPT-20B on 16 GPUs of Perlmutter

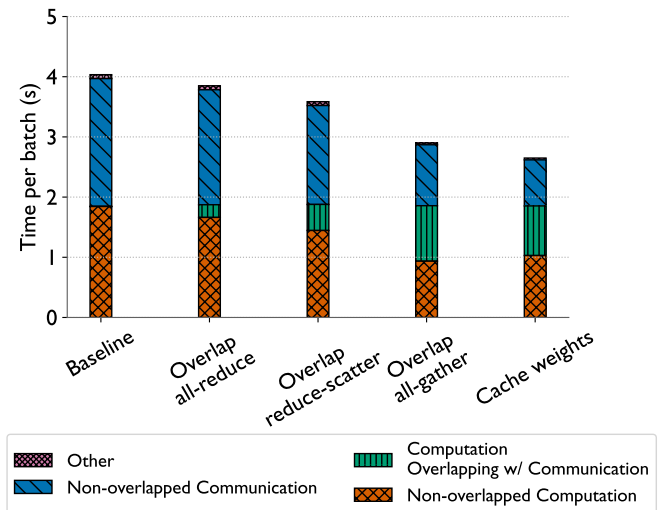


Fig. 3: Studying the effect of the proposed communication optimizations on the training times of a GPT 20B model on 16 GPUs of Perlmutter. We use Pipit [20] for creating these breakdowns from trace data collected using the PyTorch Profiler [21].

B. Overlapping Reduce-Scatters with Computation

Next we look at optimizing the reduce scatters in the backward pass (Line 12 of algorithm 1). The outputs of this reduce scatter are the gradients of the loss w.r.t. the weights of the layer. Note that these aren’t required until we have finished the backward pass of the entire network and are ready to do the all-reduces pertaining to data parallelism. Taking advantage of this we (i) issue these reduce scatters asynchronously and (ii) only wait on them to complete once all layers have finished

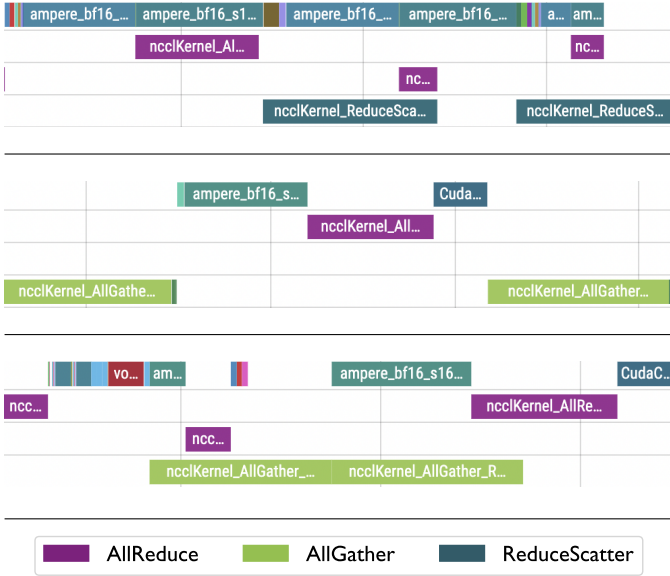


Fig. 4: PyTorch Profiler traces demonstrating i. (top) overlap of reduce scatters with backward pass compute as discussed in Section IV-B, ii. (middle) all-gathers without any overlap in the forward pass, and iii. (bottom) all-gathers after introducing the overlap optimization in Section IV-C. The first row in every trace corresponds to the compute stream and the others are communication streams.

their backward pass. This allows us to overlap the reduce scatter of one layer with the backward pass compute of its predecessors. From Figure 3, we can see that adding this optimization further increases the communication-computation overlap and improves batch times by 8%. Figure 4 (top) shows a PyTorch Profiler trace demonstrating that our optimization indeed leads to overlap of reduce-scatters with computation.

C. Overlapping All-Gathers with Computation

Our next optimization aims to overlap the all-gather operations in the forward pass (Line 2 of Algorithm 1) with computation. It’s important to note that this all-gather operation doesn’t depend on any intermediate outputs of the forward pass. Leveraging this independent nature of the all-gather, we propose to preemptively enqueue the all-gather operation for the next layer while the computation for the current layer is ongoing. At the outset of training, we generate a topological sort of the neural network computation graph to determine the sequence for performing the all-gathers. Subsequently, we execute them preemptively as outlined earlier. In Figure 3, we observe that overlapping the all-gathers in this fashion leads to even more communication-computation overlap and significant improvement to batch times of nearly 19%! Figure 4 shows a PyTorch Profiler trace without (middle) and with (bottom) this optimization, evidently showing the overlap of all-gathers with forward pass compute when the optimization is applied.

D. Caching Outputs of All-Gathers

Finally, we exploit the fact that most large scale training runs involve activation checkpointing [22], which basically is a method to significantly reduce activation memory usage albeit at an effective cost of an extra forward pass through the network. Since the parameters across the two forward passes are not changing, the all-gathers in line 2 produces the same output in the two forward passes. To eliminate the second all-gather we propose to cache the outputs of the first all-gather in the GPU memory, and reuse them during the second forward pass. For our running example of the 20B model, we cache the all-gather outputs of 28 out of the 32 transformer encoder layers and observe an improvement of nearly 9%. Overall, the four optimizations proposed in this section improve the batch times by a significant 34%!

V. A PERFORMANCE MODEL OF COLLECTIVE COMMUNICATION IN PARALLEL TRAINING

In this section, we address the following question: *how can we configure the four dimensions (i.e. G_x, G_y, G_z, G_{data}) of our 4D algorithm to minimize total communication time for a given training task?* To streamline this process for the end-user, we develop a performance model that predicts communication time based on the neural network architecture, training hyper-parameters, the four configurable performance parameters, and network bandwidths. This model returns a small set of near-optimal configurations to the user, significantly reducing the time needed to discover such configurations when compared to an exhaustive sweep of the 4D search space.

A. Placement-agnostic Performance Model

As detailed in Algorithm 1, our proposed approach relies on several collective communication operations, namely all-reduces, reduce-scatters, and all-gathers, thus we focus on predicting their times. Now, let us begin by discussing the assumptions we make in our communication model.

- *Assumption-1:* The underlying communication libraries use the bandwidth-optimal ring algorithm [23], [24] for all-reduce, reduce-scatter, and all-gather collectives. Note that the ring algorithm is a readily available option within the NCCL (NVIDIA) and RCCL (AMD) libraries.
- *Assumption-2:* For inter-node collectives, the ring is formed such that the number of ring links crossing node boundaries is minimized.
- *Assumption-3:* The message sizes are large enough such that the message startup overheads can be ignored.
- *Assumption-4:* We are only modeling the communication times and ignore the effects of any computation taking place on the GPUs.
- *Assumption-5:* We assume the same peer-to-peer bidirectional bandwidth, β_{inter} , between every pair of nodes. Similarly, we assume β_{intra} to be the peer-to-peer bandwidth between two GPUs within a node.

Let us assume that G is the number of GPUs, β is the peer-to-peer network bandwidth, and m is the size of the input buffers being sent from each GPU. We can write the message

transmission times for all-gather (t_{AG}), reduce-scatter (t_{RS}), and all-reduce (t_{AR}) as follows:

$$t_{AG} = \frac{1}{\beta} \times (G - 1) \times m \quad (1)$$

$$t_{RS} = \frac{1}{\beta} \times \left(\frac{G - 1}{G} \right) \times m \quad (2)$$

$$t_{AR} = \frac{2}{\beta} \times \left(\frac{G - 1}{G} \right) \times m \quad (3)$$

Note that these equations are adapted from the discussion on ring algorithms in Thakur et al. [23] and Rabenseifner [24], wherein we ignore the latency and computation costs in line with our assumptions.

Next, we will use these equations to estimate the time spent in communication by our 4D algorithm. Let $t_{AG,z}$ denote the time spent in the all-gather across the Z -tensor parallel groups (line 2 of Algorithm 1). Similarly, we use $t_{RS,z}$, $t_{AR,y}$ and $t_{AR,x}$ to refer to the time spent in the collectives in lines 12, 4, and 11 respectively. Similarly, we use $t_{AR,data}$ for the time spent in the data parallel all-reduce. Substituting the values of m and G for these operations in Equations 1 to 3 yields:

$$t_{AG,z} = \frac{1}{\beta} \times (G_z - 1) \times \frac{k \times n}{G_x \times G_y \times G_z} \quad (4)$$

$$t_{RS,z} = \frac{1}{\beta} \times \left(\frac{G_z - 1}{G_z} \right) \times \frac{k \times n}{G_x \times G_y} \quad (5)$$

$$t_{AR,y} = \frac{2}{\beta} \times \left(\frac{G_y - 1}{G_y} \right) \times \frac{m \times n}{G_z \times G_x} \quad (6)$$

$$t_{AR,x} = \frac{2}{\beta} \times \left(\frac{G_x - 1}{G_x} \right) \times \frac{m \times k}{G_z \times G_y} \quad (7)$$

$$t_{AR,data} = \frac{2}{\beta} \times \left(\frac{G_{data} - 1}{G_{data}} \right) \times \frac{k \times n}{G_x \times G_y \times G_z} \quad (8)$$

The total communication time for a single layer, t_{comm} is simply the sum of Equations 4 through 8:

$$t_{comm} = t_{AG,z} + t_{RS,z} + t_{AR,y} + t_{AR,x} + t_{AR,data} \quad (9)$$

For layers with ‘transposed’ weight matrices as discussed at the end of Section III, we need to swap the values of G_x and G_y , and β_x and β_y . And finally to model the communication time for the entire model, we apply Equation 9 to all of its layers, and take a sum of the times.

B. Placement-aware Performance Model

In the previous section, we made a simplifying assumption that all collectives in our hybrid parallel method have the same peer-to-peer bandwidth, denoted by β . However, the actual bandwidth available for communication between peers depends on how we map the process groups of our 4D parallel algorithm onto the underlying topology. For example,

process groups that are contained entirely within a node can experience higher bandwidths than those containing GPUs on different nodes. In this section, we attempt to model the specific bandwidths in Equations 4 through 8, given β_{inter} and β_{intra} . β_{inter} is the peer-to-peer bandwidth between two GPUs on different nodes (see Assumption 5 at the beginning of this section); β_{intra} is the bandwidth within-node.

To model the process group bandwidths, we begin by assuming a hierarchical organization of process groups: X -tensor parallelism (innermost), followed by Y -tensor parallelism, Z -tensor parallelism, and data parallelism (outermost). As a concrete example, if we have eight GPUs, and set $G_x = G_y = G_z = G_{data} = 2$, then the X -tensor parallel groups comprise of GPU pairs (0,1), (2,3), (4,5), and (6,7). Similarly, the Y -tensor parallel groups would comprise of GPU pairs (0,2), (1,3), (4,6), and (5,7), and so on.

Now let $\vec{G} = (G_x, G_y, G_z, G_{data})$ be the tuple of our configurable performance parameters, arranged in order of the assumed hierarchy. Let $\vec{\beta} = (\beta_x, \beta_y, \beta_z, \beta_{data})$ be the effective peer-to-peer bandwidths for collectives issued within these process groups. We use $\vec{\beta}_i$ and \vec{G}_i to represent the i^{th} elements of these tuples ($0 \leq i \leq 3$). Also, let G_{node} refer to the number of GPUs per node. Now let us attempt to model each β_i i.e. the bandwidth available to the GPUs in the process groups at the i^{th} level of the hierarchy.

1) *Case 1: GPUs in the process group lie within a node:*

In terms of our notation, this is the scenario when $\prod_{j=0}^i G_j \leq G_{node}$. In this case we simply use β_{intra} as the value for β_i .

2) *Case 2: GPUs in the process group are on different nodes:* In terms of our notation, this is the scenario when $\prod_{j=0}^i G_j > G_{node}$. Let us understand this case with two illustrative examples.

In Figure 5, we demonstrate a scenario with a single process group spanning eight GPUs on two nodes, with four GPUs on each node. In this case, the ring links crossing node boundaries (i.e. the link between GPUs 1 and 4, and the link between GPUs 6 and 3) will be the communication bottleneck. Since we assumed β_{inter} to be the bidirectional bandwidth between node pairs, we can set $\beta_i = \beta_{inter}$.

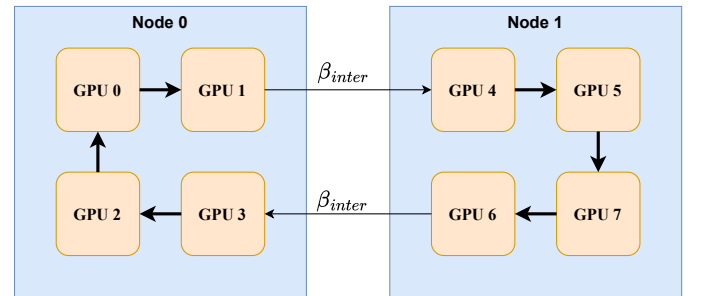


Fig. 5: Collective communication operations (all-reduce/reduce-scatter/all-gather) using the ring algorithm, spanning eight GPUs on two nodes.

Another possible scenario is when there are multiple simultaneous collectives taking place between two nodes. For

example, consider Figure 6, wherein GPUs (0, 4, 6, 2) and GPUs (1, 5, 7, 3) are executing two collectives with the ring algorithm simultaneously. In this case, the available inter-node bandwidth will be shared between these two collectives and $\beta_i = \frac{\beta_{inter}}{2}$.

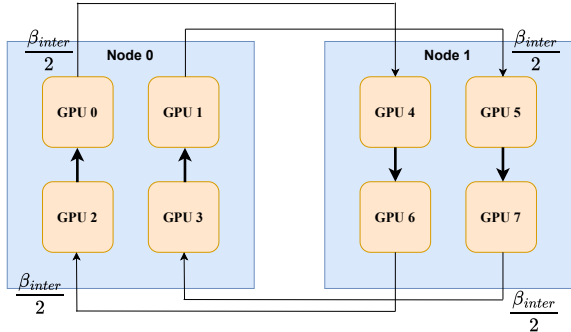


Fig. 6: Two simultaneous communication operations (all-reduce/reduce-scatter/all-gather) using the ring algorithm, each spanning four GPUs.

The first scenario occurs in the case when the process groups preceding the i^{th} process group in the hierarchy are of size one, i.e. $G_j = 1 \forall j < i$. Whereas the second scenario occurs in the case when at least one of these preceding process groups is of a size > 1 . In that case, we get multiple ring links crossing node boundaries and the bandwidth gets divided between the rings. However, note that the maximum reduction in the bandwidth is bounded by the total number of GPUs on each node, as there can't be more inter-node ring links than GPUs on a node. Equation 10 models all the scenarios to obtain the observed bandwidth:

$$\vec{\beta}_i = \frac{\beta_{inter}}{\min\left(G_{node}, \prod_{j=0}^{i-1} G_j\right)} \quad (10)$$

When we use this bandwidth term in our model, we refer to it as the placement-aware performance model.

C. Validating the Performance Models

To compare the two performance models, we collect the batch times for all possible parallel configurations of AxoNN when training GPT-20B on 32 GPUs on Perlmutter. We classify the top five configurations with respect to the batch times as ‘efficient’ and the rest as ‘inefficient’. We then rank these configurations using both the placement-agnostic (setting all bandwidths to a constant value) and placement-aware performance models. In Figure 7, we show the empirical batch times with respect to the configurations ranked by the placement-agnostic version (left) and the placement-aware version (right) of our model. Notice how four out of the top five configurations identified by the placement-aware model are ‘efficient’, while the placement-agnostic model only recognizes two. Additionally, the optimal configuration ranks first in the placement-aware model but twelfth in the placement-agnostic model. This experiment demonstrates the

utility of modeling the network bandwidths in our communication model, as well as the effectiveness of the placement-aware model in identifying efficient configurations.

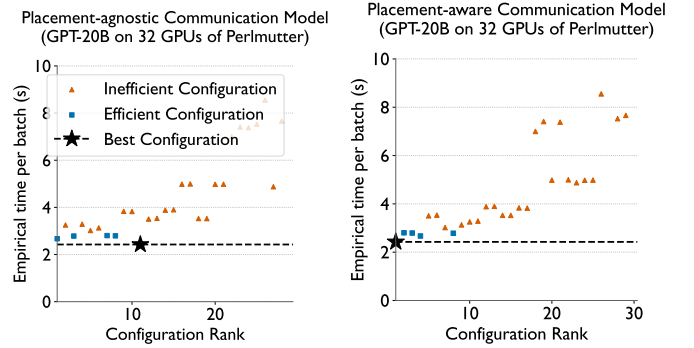


Fig. 7: Comparison of empirical batch times across different configurations, ranked by both placement-agnostic (left) and placement-aware communication models (right).

VI. EXPERIMENTAL SETUP

This section provides a detailed account of our empirical evaluation of the proposed 4D hybrid parallel algorithm which we have integrated in AxoNN. Our experiments were conducted on two supercomputers, Perlmutter and Frontier. On Perlmutter, each node is equipped with four NVIDIA A100 GPUs, each with a DRAM capacity of 40GB. Whereas on Frontier, each node has four AMD Instinct MI250X GPUs each with a DRAM capacity of 128GB. Each MI250X GPU is partitioned into two Graphic Compute Dies (GCDs) and each GCD appears as a separate device to any deep learning framework. Nodes on both systems have four HPE Slingshot 11 NICs, with each NIC capable of link speeds of 200 Gb/s.

A. Description of Neural Networks and Hyper-parameters

We evaluate the effectiveness of our proposed framework by conducting experiments on two well-known neural network architectures: U-Net [25] and GPT [3]. U-Nets are fully convolutional neural networks that have diverse applications in various fields such as text-to-image systems (e.g., Dall-E-2 [26] and Stable-Diffusion [27]), image segmentation [28], and object detection [29]. The GPT architecture is a popular transformer architecture [30] that has been used to develop several large language models [3], [4], [31], [32]. Tables I and II detail the model architectures and their corresponding hyperparameters. Due to the extremely large activation memory requirements of training GPT models, we turn on activation checkpointing [22]. Additionally, we employ mixed precision (bf16/fp32) for all our training runs.

To create parallel implementation of these architectures with AxoNN, we started with established sequential implementation. For U-Nets, we parallelized Nichol et al.’s sequential implementation [33] using our 4D approach. For transformers on Perlmutter, we leveraged the optimized sequential code from the Megatron-LM codebase [34]. However, when evaluating

TABLE I: Architectural details of the GPT-style transformers [3] that we use in this work.

Model	# Layers	Hidden-Size	# Heads
GPT-5B	24	4096	32
GPT-10B	32	5120	40
GPT-20B	32	7168	56
GPT-40B	38	9216	72
GPT-80B	42	12288	96

TABLE II: List of U-Net models [25] that we employed in our weak scaling experiments on Perlmutter. Consistent with Nichol et al. [33], our models consist of four levels, with each level comprising three residual blocks. For training, we set the batch size to 2048 and the image resolution to 32×32 .

Model	Channels	# GPUs
U-Net 250M	256	64
U-Net 500M	416	128
U-Net 1B	512	256
U-Net 2B	768	512
U-Net 4B	1024	1024

on Frontier, we encountered training instability with Megatron-LM and switched to LitGPT [35] as the foundation. We then successfully integrated our 4D algorithm as its backend.

To validate the correctness of our implementation, we train a small 50M parameter U-Net on the CIFAR-10 dataset [36] for 12,000 iterations as well as a 125M parameter GPT on the BookCorpus dataset [37] for up to 14,000 iterations and present the training losses for both of them. We then conduct weak scaling experiments with the U-Net, starting from a 250M parameter model on 64 GPUs (64 GCDs on Frontier), and scaling up to 4B parameters on 1024 GPUs (1024 GCDs on Frontier). We conduct a similar weak scaling experiment with the GPT-3 models, ranging from GPT-5B to GPT-80B on 64-1024 GPUs on Perlmutter (64-1024 GCDs on Frontier). Note that we had to make slight adjustments to layers and hidden-sizes of the GPT models listed in Table I for Megatron-LM because it requires the number of layers to be divisible by the pipeline parallelism dimension. Additionally, we conduct a strong scaling experiment for GPT-80B ranging from 64-1024 GPUs/GCDs on each supercomputer.

B. Choice of Frameworks for Comparison

We compare the performance of our proposed hybrid parallel framework with three state-of-the-art baseline frameworks: Megatron-LM [6], [34], DeepSpeed-3D [38]; ZeRO-3 [8]. Megatron-LM combines tensor, pipeline and data parallelism to efficiently train large multi-billion parameter GPT-style transformers at scale. Like Megatron-LM, DeepSpeed-3D combines data parallelism, pipeline parallelism, and tensor parallelism. ZeRO-3 is stage 3 of the ZeRO optimizer which partitions the optimizer states, gradients, and parameters across GPUs. Note that we do not run Megatron-LM on Frontier due to the training instabilities mentioned in the previous subsection. Note that since Megatron-LM and DeepSpeed-3D do not provide parallel implementations of UNets, we only

run ZeRO-3 as our baseline for the weak scaling experiments on UNets.

C. Evaluation Metrics

For our weak and strong scaling experiments we report the average time per iteration. We do so by running each framework for ten batches and reporting the average of the last five. For our GPT runs, we also calculate half precision FLOP/s using Narayanan et al.’s [34] analytical formulation for the number of floating point operations in a transformer. We then compare this number with the theoretical peaks on each machine (312 TFLOP/s per GPU on Perlmutter, and 192 TFLOP/s per GCD on Frontier) and report the achieved percentage of peak.

VII. SCALING RESULTS

In this section, we describe the results of the empirical experiments outlined in Section VI.

A. Validating Our Implementation

To establish the correctness of our implementation, we present the loss curves for a 125M parameter GPT and a 50M parameter UNet model trained on 16 GPUs using AxoNNin the left and right sides of Figure 8 respectively. For both the experiments, we set $G_x = G_y = G_z = G_{data} = 2$ so that each dimension in our algorithm is active. We also switch on all of the communication optimizations discussed in Section IV.

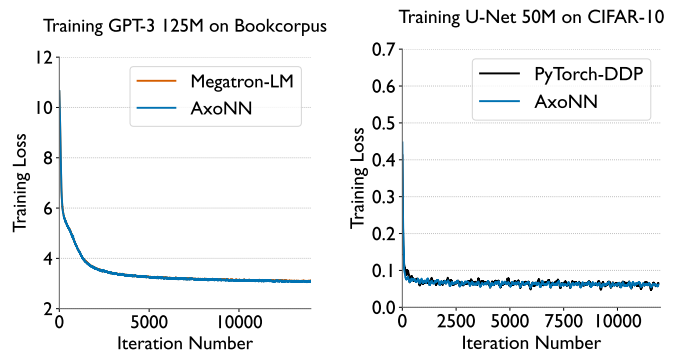


Fig. 8: Validating the correctness of our implementation by training GPT-125M and UNet-50M to completion. Details about the training hyperparameters can be found in Section VI-A.

For the GPT experiment, we compare with Megatron-LM in a pure data parallel configuration on sixteen GPUs. We observe that AxoNN successfully trains the model to convergence and produces near identical loss curves with Megatron-LM, thus validating our implementation. For the UNet experiment, we compare with PyTorch-DDP [39], which is an implementation of data parallelism native to PyTorch. Again, we observe that AxoNN successfully trains the model to convergence and produces near identical loss curves.

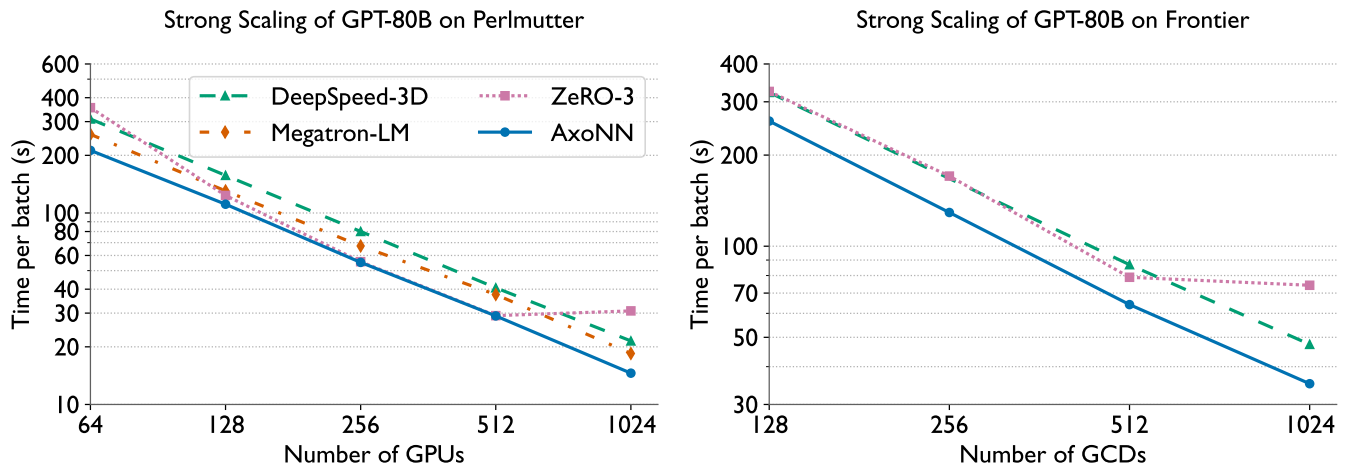


Fig. 9: Time per batch for strong scaling of GPT-80B on Perlmutter (left) and Frontier (right). We use a batch size of 4M tokens and a sequence length of 2048.

B. Strong Scaling

Next, we demonstrate the results of our strong scaling experiments on the GPT 80B architecture in Figure 9 on Perlmutter (left) and Frontier (right). On Perlmutter, we observe that AxoNN, Megatron-LM, and DeepSpeed-3D scale linearly upto 1024 GPUs. ZeRO-3 scales extremely well upto 512 GPUs matching AxoNN’s iteration times, but degrades significantly at 1024 GPUs. On 1024 GPUs, AxoNN outperforms Megatron-LM by a significant 25%, and DeepSpeed-3D by 32%! This result is particularly noteworthy considering Megatron-LM and DeepSpeed-3D, both of which combine tensor, pipeline, and data parallelism, are two of the leading approaches in parallel deep learning. Both have been instrumental in training numerous large language models (LLMs) in real-world applications [4], [31], [40], [41]. Next, let us look at the strong scaling results on Frontier (right of Figure 9). Once again we observe that ZeRO-3 does not scale beyond 512 GCDs, whereas DeepSpeed-3D and AxoNN demonstrate near linear scaling upto 1024 GCDs. On 1024 GCDs, AxoNN is faster than DeepSpeed-3D by 26% and ZeRO-3 by nearly 52%!

As established in Sections IV and V, our primary objective has been to minimize the expensive overheads of communication. To demonstrate that our performance gains stem directly from this focus, Figure 10 presents a detailed breakdown of batch times for the 80B parameter model running on 1024 GCDs of Frontier. First note that all three of AxoNN, DeepSpeed-3D, and ZeRO-3 spend nearly the same amount of time in computation - which is the sum of non-overlapped computation (red) and computation overlapped with communication (green). However, when it comes to time spent in non-overlapped communication (blue), we notice significant differences. AxoNN only spends 6 seconds of the batch time in non-overlapped communication, which is nearly 2.3× smaller than DeepSpeed-3D (15.2 seconds), and nearly 11× smaller than ZeRO-3 (74.9 seconds). This clearly demonstrates the effectiveness of our approach in minimizing communication

overheads, leading to the observed performance gains.

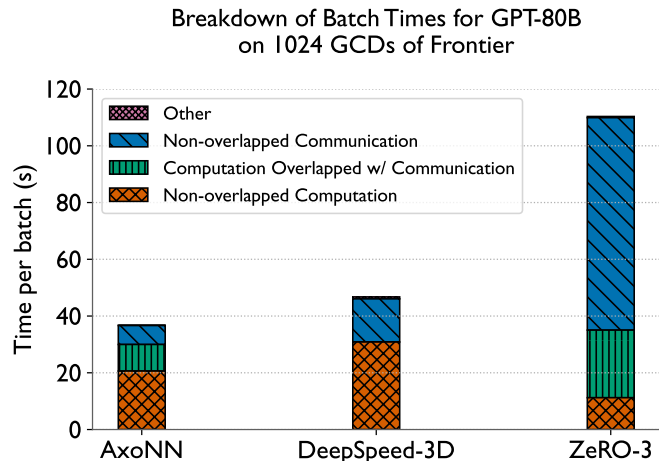


Fig. 10: Comparison of breakdown of batch times for different frameworks on a 80B GPT model run on 1024 GCDs of Frontier.

C. Weak Scaling

Now let us turn our attention to the weak scaling experiments, starting with the GPT architecture. We compare the time per iteration (or batch) for AxoNN, Megatron-LM, ZeRO-3, and DeepSpeed-3D on Perlmutter in Figure 11 (left). On Perlmutter, we observe that AxoNN has the lowest time per iteration for all models and GPU counts. For instance, AxoNN shows improvements in the range of 25–45% over Megatron-LM. For GPT 10B, 20B, and 40B, AxoNN performs better than the second best performing method ZeRO-3, with improvements in the range of 10–18%. However, similar to what we observed in our strong scaling experiments, ZeRO-3 does not scale to 1024 GPUs. At this scale, AxoNN demonstrates a 55% improvement over ZeRO-3. Figure 11 (right)

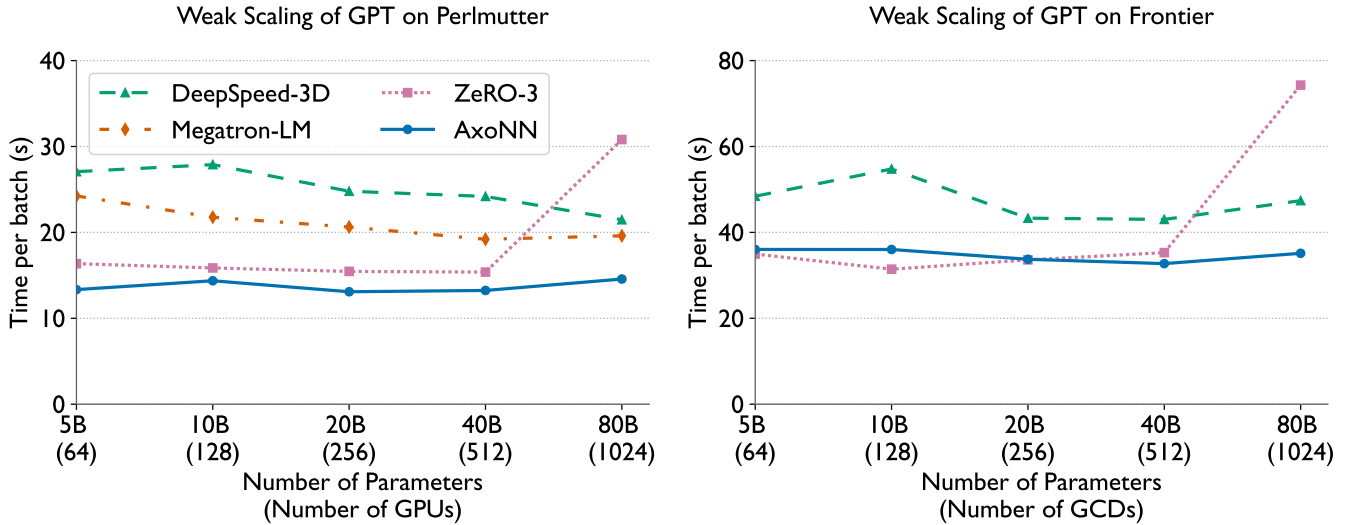


Fig. 11: Time per batch for weak scaling of GPT transformers on Perlmutter (left) and Frontier (right). We use a batch size of 4M tokens and a sequence length of 2048.

shows the performance of AxoNN, ZeRO-3, and DeepSpeed-3D on Frontier. Similar to Perlmutter, AxoNN demonstrates the lowest time per iteration for all models and GPU counts on Frontier for GPT 40B, and 80B. For GPT 5B, 10B, and 20B, ZeRO-3 outperforms AxoNN by a small margin. However, with increasing GPU counts, ZeRO-3 stops scaling efficiently, while AxoNN continues to scale efficiently. In terms of scaling, AxoNN is the best performing method for all models and GPU counts on Perlmutter and Frontier, followed by Megatron-LM on Perlmutter and DeepSpeed on Frontier.

TABLE III: Hardware flop/s utilization for weak scaling of GPTs on Perlmutter.

#GPUs	Model	Megatron-LM	ZeRO-3	DeepSpeed-3D	AxoNN
64	GPT-5B	37%	55%	33%	67%
128	GPT-10B	42%	57%	33%	63%
256	GPT-20B	42%	57%	35%	67%
512	GPT-40B	44%	55%	35%	64%
1024	GPT-80B	42%	27%	38%	57%

Table III lists the hardware flop/s utilization for the weak scaling of GPTs on Perlmutter. We notice that AxoNN demonstrates the highest utilization for almost all models and GPU counts, with a significantly high 57% of the peak half precision flop/s at 1024 GPUs of Perlmutter, which is nearly 16% of the machine! This is much higher than the next fastest framework - Megatron-LM, which clocks a significantly lower 42% of the peak.

Now, we turn our attention to the Figure 12 which shows the weak scaling performance of AxoNN and ZeRO-3 for U-Nets on Perlmutter and Frontier. Again, we observe that AxoNN is significantly faster than ZeRO-3 for all U-Net models and GPU counts. On higher GPU counts of 512 and 1024, AxoNN is up to 5 times faster than ZeRO-3 on both machines.

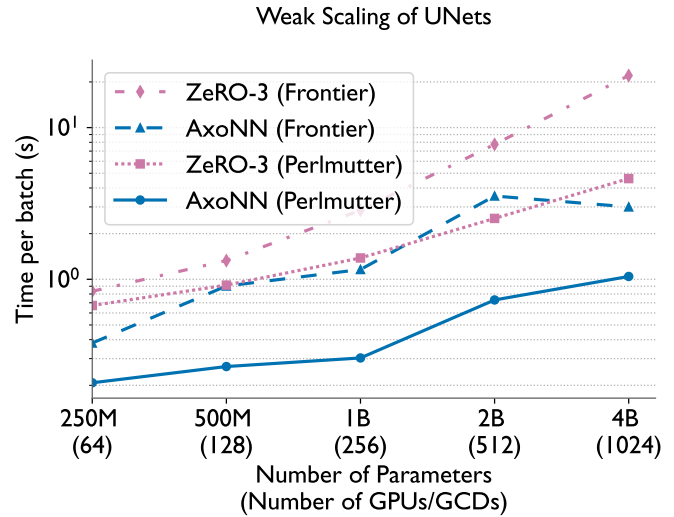


Fig. 12: Time per batch for weak scaling of UNets on Perlmutter and Frontier. We use a batch size of 2048 samples.

VIII. CONCLUSION

To overcome communication overheads in parallel deep learning, we introduced a communication-efficient four-dimensional (4D) hybrid parallel algorithm which leverages a variation of Agarwal et al.'s 3D parallel matrix multiplication algorithm [5], but goes beyond that by employing a two-pronged approach for communication efficiency. Firstly, we proposed communication optimizations that exploit asynchronous communication. This allows for significant overlap between communication and computation, maximizing hardware utilization during training. Secondly, we introduced a communication model that identifies a small set

of communication-optimal configurations for our approach. By combining an efficient parallelization approach with these communication-centric strategies, AxoNNOffers a significant step forward in tackling the communication bottleneck and enabling efficient large-scale training of neural networks.

REFERENCES

- [1] M. Belkin, D. Hsu, S. Ma, and S. Mandal, "Reconciling modern machine-learning practice and the classical bias-variance trade-off," *Proceedings of the National Academy of Sciences*, vol. 116, no. 32, pp. 15 849–15 854, 2019. [Online]. Available: <https://www.pnas.org/doi/abs/10.1073/pnas.1903070116>
- [2] J. Kaplan, S. McCandlish, T. Henighan, T. B. Brown, B. Chess, R. Child, S. Gray, A. Radford, J. Wu, and D. Amodei, "Scaling laws for neural language models," 2020. [Online]. Available: <https://arxiv.org/abs/2001.08361>
- [3] T. B. Brown *et al.*, "Language models are few-shot learners," *CoRR*, vol. abs/2005.14165, 2020. [Online]. Available: <https://arxiv.org/abs/2005.14165>
- [4] S. Smith, M. Patwary, B. Norick, P. LeGresley, S. Rajbhandari, J. Casper, Z. Liu, S. Prabhume, G. Zerveas, V. Korthikanti, E. Zhang, R. Child, R. Y. Aminabadi, J. Bernauer, X. Song, M. Shoeybi, Y. He, M. Houston, S. Tiwary, and B. Catanzaro, "Using deepspeed and megatron to train megatron-turing nlg 530b, a large-scale generative language model," 2022.
- [5] R. C. Agarwal, S. M. Balle, F. G. Gustavson, M. Joshi, and P. Palkar, "A three-dimensional approach to parallel matrix multiplication," *IBM Journal of Research and Development*, vol. 39, no. 5, pp. 575–582, 1995.
- [6] M. Shoeybi, M. Patwary, R. Puri, P. LeGresley, J. Casper, and B. Catanzaro, "Megatron-lm: Training multi-billion parameter language models using model parallelism," 2020.
- [7] Microsoft, "3d parallelism with megatronlm and zero redundancy optimizer," https://github.com/microsoft/DeepSpeedExamples/tree/master/Megatron-LM-v1.1.5-3D_parallelism, 2021.
- [8] S. Rajbhandari, J. Rasley, O. Ruwase, and Y. He, "Zero: Memory optimizations toward training trillion parameter models," in *Proceedings of the International Conference for High Performance Computing, Networking, Storage and Analysis*, ser. SC '20. IEEE Press, 2020.
- [9] Q. Xu, S. Li, C. Gong, and Y. You, "An efficient 2d method for training super-large deep learning models," 2021. [Online]. Available: <https://arxiv.org/abs/2104.05343>
- [10] B. Wang, Q. Xu, Z. Bian, and Y. You, "Tesseract: Parallelize the tensor parallelism efficiently," in *Proceedings of the 51st International Conference on Parallel Processing*. ACM, aug 2022.
- [11] Z. Bian, Q. Xu, B. Wang, and Y. You, "Maximizing parallelism in distributed training for huge neural networks," 2021. [Online]. Available: <https://arxiv.org/abs/2105.14450>
- [12] A. Jangda, J. Huang, G. Liu, A. H. N. Sabet, S. Maleki, Y. Miao, M. Musuvathi, T. Mytkowicz, and O. Sarikivi, "Breaking the computation and communication abstraction barrier in distributed machine learning workloads," 2022.
- [13] N. Dryden, N. Maruyama, T. Moon, T. Benson, M. Snir, and B. Van Essen, "Channel and filter parallelism for large-scale cnn training," in *Proceedings of the International Conference for High Performance Computing, Networking, Storage and Analysis*, ser. SC '19. New York, NY, USA: Association for Computing Machinery, 2019. [Online]. Available: <https://doi.org/10.1145/3295500.3356207>
- [14] S. Wang, J. Wei, A. Sabne, A. Davis, B. Ilbeyi, B. Hechtman, D. Chen, K. S. Murthy, M. Maggioni, Q. Zhang, S. Kumar, T. Guo, Y. Xu, and Z. Zhou, "Overlap communication with dependent computation via decomposition in large deep learning models," in *Proceedings of the 28th ACM International Conference on Architectural Support for Programming Languages and Operating Systems, Volume 1*, ser. ASPLOS 2023. New York, NY, USA: Association for Computing Machinery, 2022, p. 93–106. [Online]. Available: <https://doi.org/10.1145/3567955.3567959>
- [15] Z. Lai, S. Li, X. Tang, K. Ge, W. Liu, Y. Duan, L. Qiao, and D. Li, "Merak: An efficient distributed dnn training framework with automated 3d parallelism for giant foundation models," *IEEE Transactions on Parallel and Distributed Systems*, vol. 34, no. 5, pp. 1466–1478, 2023.
- [16] S. Li, Z. Lai, Y. Hao, W. Liu, K. Ge, X. Deng, D. Li, and K. Lu, "Automated tensor model parallelism with overlapped communication for efficient foundation model training," *arXiv preprint arXiv:2305.16121*, 2023.
- [17] L. Zheng, Z. Li, H. Zhang, Y. Zhuang, Z. Chen, Y. Huang, Y. Wang, Y. Xu, D. Zhuo, J. E. Gonzalez, and I. Stoica, "Alpa: Automating inter- and intra-operator parallelism for distributed deep learning," *CoRR*, vol. abs/2201.12023, 2022.
- [18] S. Cheng, Z. Liu, J. Du, and Y. You, "Atp: Adaptive tensor parallelism for foundation models," *arXiv preprint arXiv:2301.08658*, 2023.
- [19] A. Tripathy, K. Yelick, and A. Buluç, "Reducing communication in graph neural network training," in *SC20: International Conference for High Performance Computing, Networking, Storage and Analysis*. IEEE, 2020, pp. 1–14.
- [20] A. Bhatele, R. Dhakal, A. Movsesyan, A. Ranjan, J. Marry, and O. Cankur, "Pipit: Enabling programmatic analysis of parallel execution traces," 2023.
- [21] Meta, "Pytorch profiler," https://pytorch.org/tutorials/recipes/recipes/profiler_recipe.html.
- [22] T. Chen, B. Xu, C. Zhang, and C. Guestrin, "Training deep nets with sublinear memory cost," 2016.
- [23] R. Thakur and W. D. Gropp, "Improving the performance of collective operations in mpich," in *Recent Advances in Parallel Virtual Machine and Message Passing Interface*, J. Dongarra, D. Laforenza, and S. Orlando, Eds. Berlin, Heidelberg: Springer Berlin Heidelberg, 2003, pp. 257–267.
- [24] R. Rabenseifner, "Optimization of collective reduction operations," in *Computational Science - ICCS 2004*, M. Bubak, G. D. van Albada, P. M. A. Sloot, and J. Dongarra, Eds. Berlin, Heidelberg: Springer Berlin Heidelberg, 2004, pp. 1–9.
- [25] O. Ronneberger, P. Fischer, and T. Brox, "U-net: Convolutional networks for biomedical image segmentation," 2015. [Online]. Available: <https://arxiv.org/abs/1505.04597>
- [26] A. Ramesh, P. Dhariwal, A. Nichol, C. Chu, and M. Chen, "Hierarchical text-conditional image generation with clip latents," 2022. [Online]. Available: <https://arxiv.org/abs/2204.06125>
- [27] R. Rombach, A. Blattmann, D. Lorenz, P. Esser, and B. Ommer, "High-resolution image synthesis with latent diffusion models," 2021. [Online]. Available: <https://arxiv.org/abs/2112.10752>
- [28] S. Minaee, Y. Boykov, F. Porikli, A. Plaza, N. Kehtarnavaz, and D. Terzopoulos, "Image segmentation using deep learning: A survey," *IEEE Transactions on Pattern Analysis and Machine Intelligence*, vol. 44, no. 7, pp. 3523–3542, 2022.
- [29] L. Jiao, F. Zhang, F. Liu, S. Yang, L. Li, Z. Feng, and R. Qu, "A survey of deep learning-based object detection," *IEEE Access*, vol. 7, pp. 128 837–128 868, 2019. [Online]. Available: <https://doi.org/10.1109/2FAccess.2019.2939201>
- [30] A. Vaswani, N. Shazeer, N. Parmar, J. Uszkoreit, L. Jones, A. N. Gomez, L. Kaiser, and I. Polosukhin, "Attention is all you need," *CoRR*, vol. abs/1706.03762, 2017. [Online]. Available: <http://arxiv.org/abs/1706.03762>
- [31] BigScience, "Bigscience large open-science open-access multilingual language model," <https://huggingface.co/bigscience/bloom>, 2022.
- [32] A. Radford, J. Wu, R. Child, D. Luan, D. Amodei, and I. Sutskever, "Language models are unsupervised multitask learners," 2019.
- [33] A. Nichol and P. Dhariwal, "Improved denoising diffusion probabilistic models," 2021.
- [34] D. Narayanan, M. Shoeybi, J. Casper, P. LeGresley, M. Patwary, V. Korthikanti, D. Vainbrand, P. Kashinkunti, J. Bernauer, B. Catanzaro, A. Phanishayee, and M. Zaharia, "Efficient large-scale language model training on GPU clusters," *CoRR*, vol. abs/2104.04473, 2021.
- [35] L. AI, "Litgpt," <https://github.com/Lightning-AI/litgpt>, 2023.
- [36] A. Krizhevsky, V. Nair, and G. Hinton, "Cifar-10 (canadian institute for advanced research)." [Online]. Available: <http://www.cs.toronto.edu/~kriz/cifar.html>
- [37] Y. Zhu, R. Kiros, R. Zemel, R. Salakhutdinov, R. Urtasun, A. Torralba, and S. Fidler, "Aligning books and movies: Towards story-like visual explanations by watching movies and reading books," in *arXiv preprint arXiv:1506.06724*, 2015.
- [38] Microsoft, "Deepspeed: Extreme-scale model training for everyone," <https://www.microsoft.com/en-us/research/blog/deepspeed-extreme-scale-model-training-for-everyone/>.
- [39] S. Li, Y. Zhao, R. Varma, O. Salpekar, P. Noordhuis, T. Li, A. Paszke, J. Smith, B. Vaughan, P. Damania, and S. Chintala, "Pytorch

distributed: Experiences on accelerating data parallel training,” *Proc. VLDB Endow.*, vol. 13, no. 12, p. 3005–3018, Aug. 2020. [Online]. Available: <https://doi.org/10.14778/3415478.3415530>

- [40] J. Parmar, S. Prabhume, J. Jennings, M. Patwary, S. Subramanian, D. Su, C. Zhu, D. Narayanan, A. Jhunjhunwala, A. Dattagupta, V. Jawa, J. Liu, A. Mahabaleshwar, O. Nitski, A. Brundyn, J. Maki, M. Martinez, J. You, J. Kamalu, P. LeGresley, D. Fridman, J. Casper, A. Aithal, O. Kuchaiev, M. Shoeybi, J. Cohen, and B. Catanzaro, “Nemotron-4 15b technical report,” 2024.
- [41] S. Black, S. Biderman, E. Hallahan, Q. Anthony, L. Gao, L. Golding, H. He, C. Leahy, K. McDonell, J. Phang, M. Pieler, U. S. Prashanth, S. Purohit, L. Reynolds, J. Tow, B. Wang, and S. Weinbach, “GPT-NeoX-20B: An open-source autoregressive language model,” in *Proceedings of BigScience Episode #5 – Workshop on Challenges & Perspectives in Creating Large Language Models*, A. Fan, S. Ilic, T. Wolf, and M. Gallé, Eds. virtual+Dublin: Association for Computational Linguistics, May 2022, pp. 95–136. [Online]. Available: <https://aclanthology.org/2022.bigscience-1.9>